# Behaviour of Biomass Particles in a Bubbling Fluidized Bed: A Comparison between Wood Pellets and Wood Chips

**Article** · May 2019

DOI: 10.1016/j.cej.2019.01.120



**4 authors**, including:

Cornelius Agu
University of South-Eastern Norway
**19** PUBLICATIONS **42** CITATIONS

SEE PROFILE

Lars-André Tokheim
University College of Southeast Norway, Porsgrunn, Norway
**65** PUBLICATIONS **216** CITATIONS

SEE PROFILE

Christoph Pfeifer
University of Natural Resources and Life Sciences Vienna
**97** PUBLICATIONS **1,807** CITATIONS

SEE PROFILE

Chemical Engineering Journal 363 (2019) 84–98

Contents lists available at ScienceDirect

Chemical Engineering Journal

journal homepage: www.elsevier.com/locate/cej

# Behaviour of biomass particles in a bubbling fluidized bed: A comparison between wood pellets and wood chips

Cornelius Emeka Agu[a,*], Lars-Andre Tokheim[a], Christoph Pfeifer[b], Britt M.E. Moldestad[a]

[a] Department of Process, Energy and Environmental Technology, University of South-Eastern Norway, 3918 Porsgrunn, Norway
[b] Department of Material Sciences and Process Engineering, University of Natural Resources and Life Sciences, 1190 Vienna, Austria

## HIGHLIGHTS

- Wood pellets segregate downwards while chips upwards at low gas velocities.
- Spreads to the walls is better with wood chips than with pellets at the same gas velocity.
- Gas velocity required to achieve good mixing increases with biomass load.
- Transition from bubbling to slugging regime gets smoother at higher biomass load.
- A mechanistic model was developed for predicting the minimum mixing gas velocity.

## ARTICLE INFO

*Keywords:*
Segregation
Biomass
Particle mixing
Wood chips
Wood pellets

## ABSTRACT

For successful operation and design of a bubbling fluidized bed reactor handling a specific biomass, in-depth knowledge about the bed behaviour is paramount. This study compares the behaviour of a bed of sand containing wood pellets with that containing wood chips at different gas velocities and biomass proportions in a cold fluidized bed of diameter, 10.4 cm. The density and volume-equivalent spherical particle diameter of the pellets are 1139 kg/m$^3$ and 8.96 mm, respectively while those of the wood chips are 423 kg/m$^3$ and 6.87 mm, respectively. The results show that at low gas velocities, wood chips segregate upwards while the pellets segregate downwards in their respective beds. The spread of biomass towards the walls is higher in the bed with wood chips than in that with wood pellets. As the biomass load increases, the bubble diameter increases and the transition from bubbling to slugging regime gets smoother, resulting in an increase in the minimum slugging velocity. The minimum gas velocity for effective solids mixing is less dependent on the bed height, but increases with increase in the biomass load and decreases with increase in the bed diameter. However, when slugs flow in the bed, the biomass layer at the bed surface plugs, preventing mixing of particles to be achieved at the desired gas velocity. A mechanistic model is developed for predicting the minimum gas velocity required to achieve an effective mixing at the surface of a segregated bed. Although this study is conducted in a cold bed, this same model is considered important for a hot bed reactor since devolatilization enhances the upward flow of biomass due to reduction of the biomass density.

## 1. Introduction

Application of bubbling fluidized bed for gasification or combustion of biomass requires in-depth understanding of the bed behaviour at different gas velocities. Due to the peculiar properties of biomass, for example its large size, cohesiveness and irregular shape, it is often difficult to get it fluidized at the desired operating gas velocity. However, with increase in the reactor pressure or reduction of the particle size [1], the quality of biomass fluidization can be improved. The biomass fluidization quality can also be improved by applying surface coating [2] or a noise-induced mechanism such as mechanical vibration [3] and acoustic sound [4,5]. In addition to ensuring uniform heat and mass transfer, an inert material, sand for example, can be used to achieve the fluidization of biomass at the desired operating condition. However, as sand particles are usually smaller and higher in density compared to biomass, particle segregation is often a problem in

* Corresponding author.
*E-mail addresses:* cornelius.e.agu@usn.no (C.E. Agu), Lars.A.Tokheim@usn.no (L.-A. Tokheim), christoph.pfeifer@boku.ac.at (C. Pfeifer), britt.moldestad@usn.no (B.M.E. Moldestad).

https://doi.org/10.1016/j.cej.2019.01.120
Received 7 November 2018; Received in revised form 16 January 2019; Accepted 21 January 2019
Available online 22 January 2019

**Nomenclature**

| | |
|---|---|
| $A$ | bed cross-sectional area, $m^2$ |
| $A_p$ | particle total surface area, $m^2$ |
| $D$ | bed diameter, m |
| $D_b$ | bubble diameter, m |
| $d$ | diameter, m |
| $d_{p,sph}$ | spherical particle diameter, m |
| $\Delta e$ | bed expansion |
| $f_b$ | bubble frequency, $s^{-1}$ |
| $f_{wake}$ | bubble wake volume fraction |
| $G$ | volumetric bubble flux, m/s |
| $g$ | acceleration due to gravity, $m/s^2$ |
| $h$ | height, vertical position in the bed, m |
| $H$ | total bed height, m |
| $k$ | internal pressure coefficient |
| $l_{max}$ | maximum layer thickness, m |
| $m_p$ | mass of particles, kg |
| $m$, $n$ | dimensionless model coefficient |
| $N_{pix}$ | number of pixels in a bed cross section |
| $\Delta p_g$ | gas pressure drop, Pa |
| $s$ | size representative (volume, length, diameter) |
| $U$ | superficial gas velocity, m/s |
| $u_b$ | bubble velocity, m/s |
| $V$ | volume, $m^3$ |
| $\bar{V}$ | bulk volume, $m^3$ |
| $w_i$ | component weight fraction |
| $X$ | local mass fraction |
| $x$ | biomass total mass fraction |
| $Y$ | local volume fraction |
| $y$ | total volume fraction |

*Greek symbols*

| | |
|---|---|
| $\alpha$ | local solids fraction |
| $\beta$ | fluid-particle momentum transfer coefficient, $N/m^3$ |
| $\delta_b$ | bubble volume fraction |
| $\varepsilon$ | average bed void fraction |
| $\varepsilon_s$ | average solids fraction of sand bed |
| $\varepsilon_b$ | average solids fraction of biomass bed |
| $\theta_i$ | angle of internal friction, degree |
| $\sigma$ | normal stress, Pa |
| $\rho$ | density, $kg/m^3$ |
| $\bar{\rho}_p$ | particle bulk density |
| $\varphi$ | sphericity |
| $\tau_w$ | wall frictional stress, Pa |
| $\mu_w$ | wall frictional coefficient |
| $\gamma$ | hydrostatic pressure correction coefficient |

*Subscripts*

| | |
|---|---|
| b | biomass, bubble |
| bs | bubbling to slugging transition |
| f | fluidized |
| g | gas |
| i,j | indices locating a pixel |
| m | mixture |
| mf | minimum fluidization |
| p | particle |
| s | sand |
| 0 (zero) | initial state or entry position |

biomass fluidized bed reactors [6]. This study investigates the behaviour of wood-based biomass particles in fluidized beds aided by sand particles. Two different types of woody biomass: wood chips and wood pellets are investigated and their behaviour in bubbling fluidized beds are compared. Both types of biomass are widely utilized due to their availability and energy content. While the wood chips are lighter, have a wider variation in shape and a low unit cost (cost per kWh), the wood pellets have a lower moisture content and a higher energy density due to their relatively high mass density. The difference between the properties of the two different types of biomass may influence their behaviour in fluidized beds, and thus the choice of reactor design and operating conditions. It should be noted that in biomass fluidized bed reactors, different types of solid particles are present including bed material, raw biomass, ash and char particles, all with different physical properties.

A number of studies have investigated the fluidized bed behaviour in systems involving biomass mainly in cold flows. Measurement of minimum fluidization velocity of mixtures of biomass and inert bed materials at different biomass concentrations [4,7–9] is common. The minimum fluidization velocity increases with increase in the proportion of biomass in the bed. Different studies have also reported the segregation and mixing behaviour of biomass-sand mixtures at higher gas velocity using different measurement techniques. Along with the fibre optic sensors for measuring bubble properties, the most commonly used methods for the measurement of biomass distribution are the frozen bed method [10,11] and particle tracking techniques based on radioactivity [11] and magnetic fields [12]. Although the particle tracking technique requires complex analysis, it usually gives more accurate results than the frozen bed method. The accuracy of the latter depends on the biomass load in the bed [11]. Based on experimental findings, the mixing of solids is enhanced by increasing the amount of biomass in the bed [13], and the pattern of solids mixing is independent of the bed height [14]. In addition, segregation of particles in a bed increases with increase in the gas flow rate up to a certain gas velocity. Above this gas velocity, mixing of solids over the entire bed volume can be achieved [15]. Zhang et al. [15] classified the progress of a bed of a biomass-sand mixture into six stages, ranging from a well-mixed to a local-segregated state as the gas velocity is increased. Moreover, particle size, shape and densities also influence the pattern of mixing and segregation in the fluidized bed, which according to Baeyens and Geldart [16] and Yang [17] are brought about by the passage of bubbles through the bed. By using smaller or denser biomass particles, Cluet et al. [14] showed that bed homogeneity can be enhanced. When the density of the smaller particles in the mixture is higher, these particles segregate downwards at low gas velocity and upwards at high gas velocity [18]. To gain an overview of which component in a bed mixture can segregate up or down when fluidized, Di Renzo et al. [10] proposed an equilibrium model, which depends on the density and size ratios of the particles, and also on the proportion of biomass in the binary mixture.

The effects of biomass particle size and shape on the fluidized bed behaviour are reported in [8,11]. From different mixtures of biomass and 380 μm sand particles, Fotovat et al. [11] concluded that the higher the sphericity of biomass particles, the faster they rise and the slower they sink when the gas velocity is increased. The authors also showed that bubbles are more prone to break in the bed containing biomass particles with low sphericity, resulting in smaller bubbles in the bed. In addition, increasing the size and amount of biomass particles, Zhang et al. [19] showed that the probability of bubble growth in the bed mixture decreases, which leads to flow of smaller bubbles compared to that in the bed of pure sand particles.

In view of these studies, this paper is aimed at comparing the bubble-induced bed properties between a low-density ($< 500\,kg/m^3$) and high-density ($> 1000\,kg/m^3$) woody biomass in bubbling fluidized beds assisted with sand particles of density, $2650\,kg/m^3$. The pattern

and degree of segregation due to density difference between the sand and wood particles in the bed mixtures are investigated. As the required global mixing depends on the gas velocity and biomass load, this study also looks into mechanisms involved in achieving solids mixing over the biomass accumulated at the surface or at the bottom of the bed. Understanding these mechanisms can help in selecting or predicting the gas velocity required for mixing to occur over the bed height. The results presented in this study are based on measurements of solids fraction at different positions in a 10.4 cm diameter cold fluidized bed using electrical capacitance tomography (ECT) sensors. ECT measures the distribution of relative permittivity in a bed, which differs from one solid material to another. This means that the relative permittivity of a mixture of biomass and sand particles will be different from that of pure sand at the same gas velocity and bed position. Therefore, measurements of biomass distribution can be obtained by comparing the ECT data acquired from a bed mixture with those acquired from the pure sand particles under the same measurement conditions. The data from the ECT sensors are also analysed to obtain the bubble diameter, bubble frequency and volumetric bubble flux. Additionally, the segregation behaviour observed in the ECT setup is compared with that observed at different bed aspect ratios in a setup equipped with pressure sensors. In the subsequent sections, the results are presented, discussed and compared with correlations in the literature. The results obtained and described here enhance understanding of the complex fluid-particle behaviour in fluidized bed combustors and gasifiers. By using appropriate scaling laws [20] and a measured output such as the bubble to bed diameter ratio, the behaviour observed in this study can also be scaled up to larger diameter bed in a similar approach as discussed in Agu et al. [21].

## 2. Setup and measurement procedure

### 2.1. Experimental setup

Two different cold fluidized bed setups as shown in Fig. 1 were used in this study. The first of these consists of a cylindrical Perspex glass column of internal diameter 8.4 cm and height 140 cm. The column is fitted with a porous steel plate distributor of 40% flow area, and 10 different pressure sensors located along the column axis. The first sensor is located 4 cm below the gas distributor and 6.5 cm from the second sensor while the other ones are equally spaced above the distributor at 10 cm interval. Based on this setup, the minimum fluidization velocity and the corresponding void fraction of all the pure solid particles used in this study were determined.

To investigate the bubble properties in the fluidized bed of a mixture of sand and biomass particles, a setup equipped with two ECT sensors was used. The cylindrical Perspex glass column has a diameter of 10.4 cm and a height of 140 cm. The column is also equipped with a stainless steel porous plate for uniform gas distribution across the bed. The ECT sensors are located 15.7 cm and 28.7 cm above the distributor.

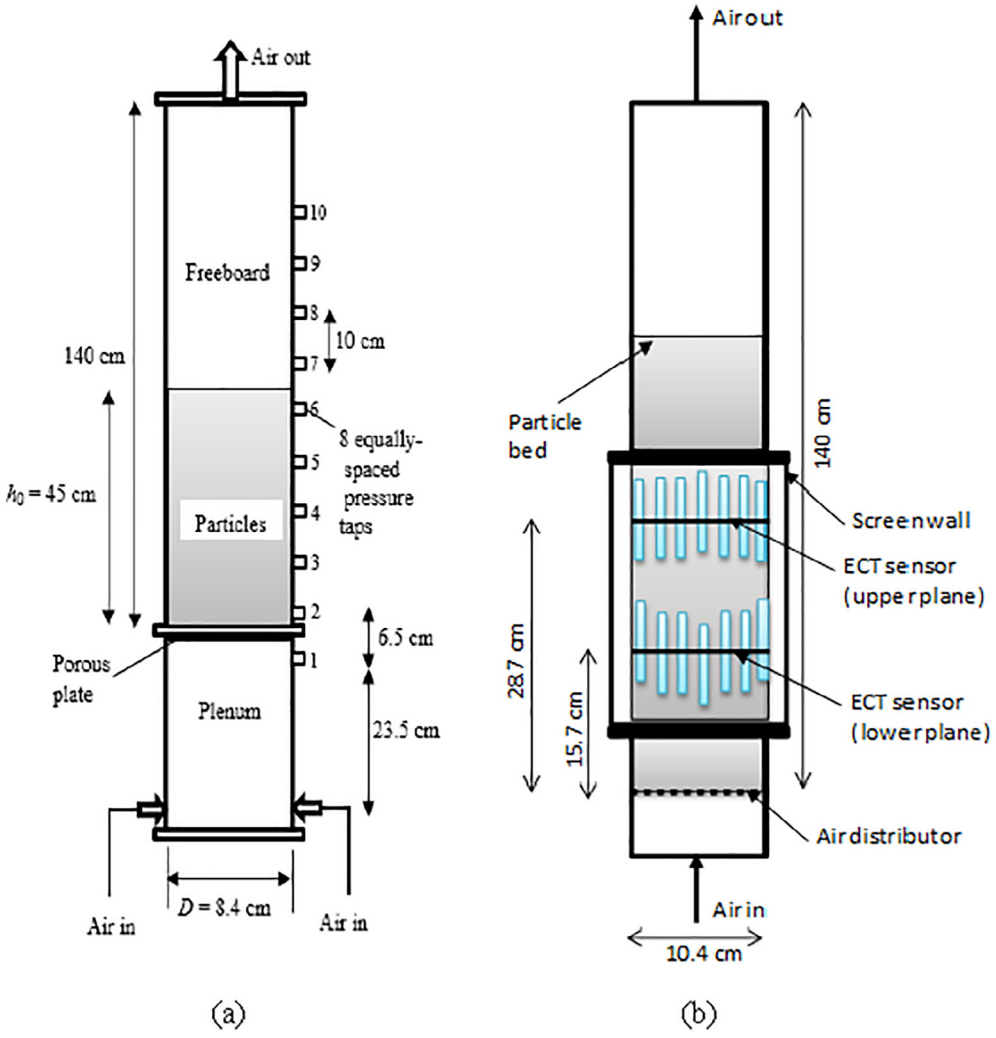


**Fig. 1.** Schematic illustration of a cold fluidized bed equipped with (a) pressure sensors for measurement of pressure drops (b) ECT sensors for measurement of solids fraction distribution.

The details of this setup and configuration of the ECT can be found in Agu et al. [22]. At a given gas flow rate, the ECT measures the distribution of solids fraction across a section of the bed. Similar to the pressure sensor setup, compressed air at the ambient condition was used at different velocities for all the beds investigated. For each gas velocity, the image data acquired by the ECT sensors were captured at a frequency of 100 Hz for 60 s. The bed height was also measured for each gas velocity when the flow had been established (approximately after 3 min) using a ruler attached to the column wall. The captured data were exported and analysed using MATLAB codes developed in-house. Different bubble properties including bubble diameter, bubble frequency and bubble volumetric flow rate were obtained from the analysis. During the data analysis, a bubble was considered as a region with a solids fraction below 0.2. The bubble properties were computed from the time evolution of the bubble-projected area. The variation of the projected area with time shows that for a given gas velocity above the minimum bubbling velocity, bubbles pass periodically across a measurement plane. The reciprocal of the time between arrivals of two successive bubbles to the plane gives the bubble frequency. By assuming a spherical bubble, the bubble diameter is determined from the peak of the projected area during each bubbling period. As there may be deviations in the bubble property measured at each bubble passage, the results reported in this study are the time-average values obtained over the 60 s measurement period. More information on measurement of bubble properties using this setup is given in Agu et al. [23].

### 2.2. Material properties and characterization

Two different types of wood-based biomass are investigated. The biomass includes cylindrical wood pellets of 6 mm diameter and wood chips with a wide variation in shape. The pellets vary in length between 5 and 30 mm. For analysis, a rectangular shape is assumed for the wood chips with variation in length, width and height in the range of 5–12 mm, 5–12 mm and 1–5 mm, respectively. The fluidized material is sand particles with a narrow size distribution (200–350 μm). The detailed properties of these materials are given in Table 1.

The void fraction of the bed is computed as

$$\varepsilon = 1 - \bar{\rho}_p/\rho_p \tag{1}$$

where $\bar{\rho}_p$ is the bulk density of the solid particles obtained as mass of the solids per unit volume of the bed, and $\rho_p$ is the particle density. The average size, $s$ (diameter, length, volume) of the particles in each bulk material is computed as

$$s = \frac{1}{\sum_i \left(\frac{w_i}{s_i}\right)} \tag{2}$$

where $s_i$ is the mean value of each size range and $w_i$ is the mass fraction of the size range in the bulk material. For the non-spherical biomass particles, the volume-equivalent spherical particle diameter, $d_{p,sph}$ is determined from:

$$d_{p,sph} = \left(\frac{6V_p}{\pi}\right)^{1/3} \tag{3}$$

where $V_p$ is the mean volume of the particle computed from Eq. (2). With the value of $d_{p,sph}$, the effective particle diameter is obtained from $d_p = \varphi_p d_{p,sph}$. The particle sphericity, $\varphi_p$, defined as the ratio of surface area of a sphere to surface area of the particle of the same volume as the spherical particle, is given by

$$\varphi_p = \frac{6\pi^{\frac{1}{3}} V_p^{\frac{2}{3}}}{A_p} \tag{4}$$

Here, $A_p$ is the mean particle surface area. The size of the sand particles was obtained from the sieve analysis and the average particle sphericity was obtained by fitting the Carman-Kozeny [24] equation with the pressure drop across a bed of these particles at different air velocities.

In addition, the minimum fluidization velocity of each material was obtained as the superficial gas velocity when the pressure drop across the bed is equal to the bed weight divided by the cross-sectional area of the bed. As can be seen in Table 1, the wood chips and pellets have close particle size but a wide density difference. The difference in density between the two different wood materials is key factor employed in this study. Moreover, the size variation of the two different biomass types also mimic those used in large-scale biomass gasifiers or combustors. The densities of both wood materials are lower than that of the sand particles, and as a result, segregation of sand and wood particles is expected to occur during fluidization as reported in previous studies [14,18].

### 2.3. Local biomass concentration

To quantify the segregation behaviour between sand and biomass particles at a given gas velocity, it is necessary to measure the distribution of biomass particles which is often present in a lesser amount. However, since no particle-tracking sensor is employed in this study, a mathematical model is needed. By comparing the volume fraction of pure sand with that of the sand-biomass mixture at the same bed position and gas velocity, it is possible to ascertain the distribution of biomass along the bed axis. For example, Fig. 2(a) compares the radial distributions of solids fraction in a bed of pure sand particles with those in a bed containing sand and 30 vol% wood pellets at different gas velocities. At the lower velocity, $U_0 = 0.06$ m/s, neither of the beds is fluidized. The higher solids fraction in the bed mixture compared to the bed of sand is due to presence of the wood particles. The relatively small amount of pellets in the bed increases the packing density of sand particles. However, at the higher gas velocity, $U_0 = 0.16$ m/s, both beds are bubbling, leading to a decrease in the solids fraction. Because biomass particles follow the path along the flow of bubbles, the concentration of biomass particles is higher near the bed axis, resulting in a stronger depression of solids fraction of the bed mixture compared to that of sand particles. It should also be noted that when a section of a bed contains nearly 100% biomass particles, the ECT sensor measures a very high relative permittivity. In this case, the solids fraction of the bed mixture becomes higher than the value at the initial state.

Assuming a linear volume combination, the time-averaged mixture solids volume fraction, $\alpha_{i,j,m}$ at a given pixel (i, j) shown in Fig. 2(b) can be expressed in terms of the corresponding pure component values as

$$\alpha_{i,j,m} = \alpha_{i,j,s} \pm \alpha_{i,j,b} \tag{5}$$

The ± sign is included since the value of $\alpha_{i,j,m}$ can be higher or lower than the solids fraction, $\alpha_{i,j,s}$, in the bed of sand particles as shown in Fig. 2(a). In relation to sand particles, the biomass solids fraction, $\alpha_{i,j,b}$ in the mixture can thus be obtained as

**Table 1**
Biomass and sand particle properties at fixed state.

| Materials | Shape | $\rho_p$ (kg/m$^3$) | $d_{p,sph}$(mm) | $\varphi_p$ (−) | $\varepsilon$ (−) | $\varepsilon_{mf}$ (−) | $U_{mf}$ (m/s) |
|---|---|---|---|---|---|---|---|
| Wood pellets | Cylindrical | 1139 | 8.96 | 0.82 | 0.43 | 0.46 | 1.99 |
| Wood chips | Rectangular | 423 | 6.87 | 0.75 | 0.49 | 0.57 | 1.27 |
| Sand | Angular | 2650 | 0.293 | 0.86 | 0.42 | 0.46 | 0.079 |

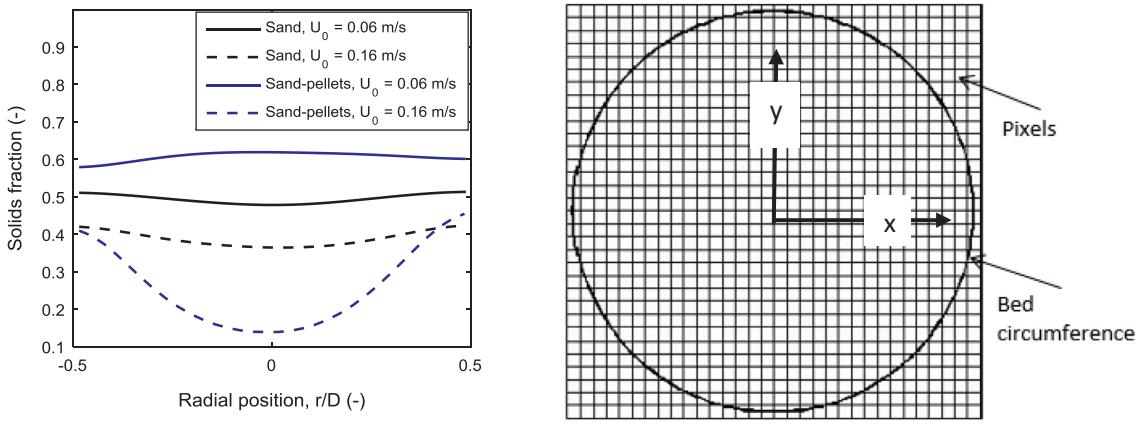


**Fig. 2.** (a) Radial distribution of solids fraction obtained from ECT at the lower plane for a bed with 30% wood pellets compared with that of pure sand particles; (b) Cross-section of the bed divided into 812 pixels.

**Table 2**
Properties of bed mixture at different biomass concentration.

| Biomass volume fraction (%) | $\varepsilon_m$ (−) | | $\rho_m$ kg/m$^3$ | | $d_m$ (mm) | |
|---|---|---|---|---|---|---|
| | Pellets | Chips | Pellets | Chips | Pellets | Chips |
| 0 | 0.448 | 0.448 | 2650 | 2650 | 0.252 | 0.252 |
| 5 | 0.427 | 0.420 | 2574 | 2539 | 0.265 | 0.265 |
| 10 | 0.404 | 0.410 | 2499 | 2427 | 0.279 | 0.279 |
| 20 | 0.388 | 0.380 | 2348 | 2205 | 0.312 | 0.311 |
| 30 | 0.353 | 0.333 | 2197 | 1982 | 0.355 | 0.352 |
| 50 | 0.258 | 0.250 | 1895 | 1537 | 0.487 | 0.481 |

$$\alpha_{i,j,b} = \alpha_{i,j,s} - \alpha_{i,j,m} \tag{6}$$

With $X_{i,j,b}$ the mass fraction of biomass in the mixture,

$$\alpha_{i,j,b} = X_{i,j,b} C_{i,j,m} / C_{i,j,b} \tag{7}$$

where $C_{i,j,b}$ is the mass concentration of biomass. The mixture mass concentration $C_{i,j,m}$ can be obtained from

$$C_{i,j,m} = \frac{\alpha_{i,j,m}}{\left(\frac{X_{i,j,b}}{\rho_b} + \frac{1 - X_{i,j,b}}{\rho_s}\right)} \tag{8}$$

Noting that $C_{i,j,s} = \alpha_{i,j,s}\rho_s$, it can be shown based on the mass balance that

$$\alpha_{i,j,b} = \frac{X_{i,j,b}}{1 - \frac{\alpha_{i,j,s}}{\alpha_{i,j,m}}\left[\left(\frac{\rho_s}{\rho_b} - 1\right)X_{i,j,b} + 1\right]} \tag{9}$$

From Eq. (9), $X_{i,j,b}$ can be obtained as

$$X_{i,j,b} = \frac{{\alpha_{i,j,b}}^2/\alpha_{i,j,m}}{1 + \frac{\alpha_{i,j,s}\alpha_{i,j,b}}{\alpha_{i,j,m}}\left(\frac{\rho_s}{\rho_b} - 1\right)}$$

$$X_{i,j,b} = \frac{(\alpha_{i,j,s} - \alpha_{i,j,m})^2}{\alpha_{i,j,m} + \alpha_{i,j,s}(\alpha_{i,j,s} - \alpha_{i,j,m})\left(\frac{\rho_s}{\rho_b} - 1\right)} \tag{10}$$

On volume basis, the biomass concentration at any position in the bed is therefore given by

$$Y_{i,j,b} = \frac{X_{i,j,b}}{X_{i,j,b} + \frac{\rho_b}{\rho_s}(1 - X_{i,j,b})} \tag{11}$$

The input parameters to Eq. (11) are the solids fraction of the pure sand particles, $\alpha_{i,j,s}$, measured at a position in the bed and the corresponding solids fraction of the biomass-sand mixture, $\alpha_{i,j,m}$, obtained at the same bed condition. For a given plane in the bed, the average volume fraction of biomass particles, $Y_b$, across the cross section of the plane can be obtained from Eq. (12), where $N_{pix} = 812$ is the total number of pixels within the bed cross section.

$$Y_b = \frac{1}{N_{pix}}\left(\sum_i \sum_j Y_{i,j,b}\right) \tag{12}$$

### 2.4. Experimental procedure

Five different mixture compositions were used for characterizing the fluidized bed behaviour. Table 2 shows the proportion of biomass and sand particles used in each mixture. For the individual mixture, the amount of material required to form the bed was divided into 10 portions, each containing the same proportion of sand and biomass particles as in the total mixture. The different portions of the mixture were charged into the column one after the other, and thereafter the column walls were properly shaken. This procedure helped to ensure that both different types of particles are sufficiently present at the measurement planes during the sensor calibration. The same total bed height, 50 cm at fixed state, was used for all mixtures. With this bed height, the aspect ratio, $h/D = 5$, is very high. There are two reasons for using this high aspect ratio: (1) To ensure that the upper ECT sensor located at a position 28.7 cm from the distributor is well-covered. With this, the signal to noise level can be minimized during the sensor calibration. (2) To enhance understanding of the behaviour of biomass-sand mixture across different bed aspect ratios since most of the previous studies are based on shallow beds. To verify the influence of bed height on the behaviour observed in this setup, the different mixtures of sand and biomass particles were fluidized at different gas velocities in the setup equipped with pressure sensors. As this setup is transparent over the entire bed height, the particle segregation patterns were clearly observed. Two different bed aspect ratios, 1.2 and 2.4, were used for this demonstration.

For prediction of different properties obtained in the binary mixtures at fluidized state, the average diameter, density and sphericity of the particles are based on the following expressions.

$$d_m = \left[\frac{y_b}{d_b} + \frac{(1 - y_b)}{d_s}\right]^{-1} \tag{13}$$

$$\rho_m = y_b\rho_b + (1 - y_b)\rho_s \tag{14}$$

$$\varphi_m = d_m/d_{p,sphm} \quad (15)$$

Here, $y_b$ is the volume fraction of biomass in the mixture while the subscripts "m", "b" and "s" denote mixture, biomass and sand, respectively. Moreover, the initial void fraction of the mixture, $\varepsilon_m$, given in Table 2 is computed based on the mixture average density obtained from Eq. (14).

## 3. Results and discussion

In this section, different bed properties due to flow of bubbles are presented. The behaviour in the bed containing wood pellets is compared with that containing an equal amount of wood chips at the same gas velocity.

Fig. 3 shows the distribution of solids fraction in the upper measurement plane for the beds containing 20 vol% of biomass particles. A high value on the figure colour bar indicates a high solids fraction. Based on the threshold solids fraction of 0.2, it can be seen that a bubble contains a central region with a gas pocket (region of no solids) surrounded by a thin region of dilute phase (solids fraction less than 0.2). The size of the bubble rising in the bed with wood chips is larger than that rising in the bed with wood pellets at the same measurement plane and gas velocity. The figure also shows that the concentration of solids increases gradually away from the bubble region. Since the solids concentration is higher in the bed of pure sand particles, this indicates that in the presence of bubbles, biomass particles are located in the dilute region of the emulsion phase of the bed (the region excluding the bubbles).

### 3.1. Transition to fluidization and slugging regimes

For each of the biomass-sand mixtures, the minimum fluidization and slugging velocities were obtained from plots of solids fraction fluctuation against superficial air velocity, as described in Agu et al. [22]. Fig. 4 shows the measured values of $U_{mf}$ and $U_{ms} - U_{mf}$ at different amounts of biomass in the mixture. As can be seen, the minimum fluidization velocity of the mixture with wood pellets slightly decreases with increase in biomass volume fraction up to 0.2. At higher biomass concentration, $U_{mf}$ increases with increase in the biomass load. Since the sand particle properties are the same, the decrease in minimum fluidization velocity at increasing amount of biomass suggests that the void fraction of the bed mixture decreases. For the case of wood chips, the value of $U_{mf}$ increases as the amount of biomass in the mixture increases due to higher void fractions of the beds. Comparing the experimental results in Fig. 4(a) with those from different correlations [4,7–9], the prediction error is as high as 40%. As illustrated, the Rao and Bheemarasetti [7] model under predicts the minimum fluidization velocity in the mixture containing up to 20% wood pellets and over predicts the fluidization velocity for higher pellets concentration. As the $U_{mf}$ values of pure wood chips and wood pellets are almost the same, the Cheung et al. [25] model predicts approximately the same value of $U_{mf}$ when $y_b < 0.3$ in these biomass beds.

In addition, Fig. 4(b) shows that the minimum excess slugging velocity, $U_{ms} - U_{mf}$, increases as the biomass volume fraction increases between 0 and 0.3. Although the $U_{ms} - U_{mf}$ value is slightly higher for the bed with pellets compared to that with wood chips of equal volume, the trend of the variation is the same for the two woody biomasses. The delay in the onset of slugging in the different bed mixtures suggests that bubble diameter decreases with increasing amount of biomass. No available correlations [23,26,27] applied in the beds of pure solid particles can appropriately predict the trend of $U_{ms} - U_{mf}$ shown in Fig. 4(b). However, analysis of the experimental data shows that the ratio $U_{ms}/U_{mss}$ is independent of the biomass type as given in Eq. (16), where $U_{mss}$ is the minimum slugging velocity of the sand particles. As shown in Fig. 4(b), Eq. (16) accurately reproduces the experimental data for the biomass loads up to 30 vol%.

$$\frac{U_{ms}}{U_{mss}} = e^{1.13y_b} \quad (16)$$

### 3.2. Effect of gas velocity on biomass distribution

The distribution of biomass in a bed mixture can be obtained using different correlations [13,28]. According to Fotovat et al. [13], the biomass volume fraction along the bed axis can be predicted as follows:

$$Y_b = \frac{(1-\delta_b)(1-\varepsilon_e)}{(1-\delta_b)(1-\varepsilon_e) + f_{wake}\delta_b(1-\varepsilon_f)} Y_{be} \quad (17)$$

where the amount of biomass, $Y_{be}$ in the emulsion phase is computed from the following equation and boundary condition (BC):

$$\frac{dY_{be}}{dh} = \frac{0.0405\delta_b(1-\varepsilon_f)A}{\varepsilon_{mf} D_b (Q_{sb} + Q_{be})} Y_{be}; \quad \text{BC:} \quad Y_{be}(h=0) = 2x_b^{1.2}U_0^{1.6} \quad (18)$$

Here, $\delta_b$ is the bubble volume fraction evaluated as the ratio of bubble volumetric flux to the bubble velocity, $\varepsilon_e$ is the void fraction in the emulsion phase, and $Q_{sb}$ and $Q_{be}$ are the volumetric flow rates of sand and biomass in the bubble and emulsion phases, respectively. $A = \pi D^2/4$, where $D$ is the bed diameter. The detailed expressions for all the necessary input to Eqs. (16 and 17) are given in [13]. For the bubble diameter, $D_b$, the model proposed by Darton et al. [29] is used

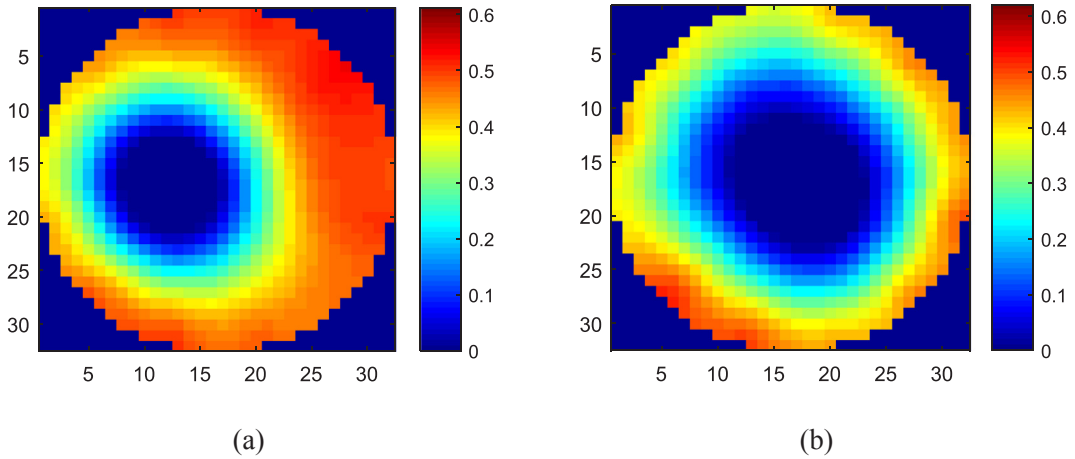


**Fig. 3.** Contour showing the distribution of solids fraction at $U_0 = 0.16$ m/s in a bed mixture of sand and 20% vol. of (a) wood pellets (b) wood chips; bed position = 28.7 cm above distributor. Solids fraction increases with the colour scale value (deep blue (0) = only air; deep red (0.6) = only solid; between 0 and 1 = air–solid mixture).

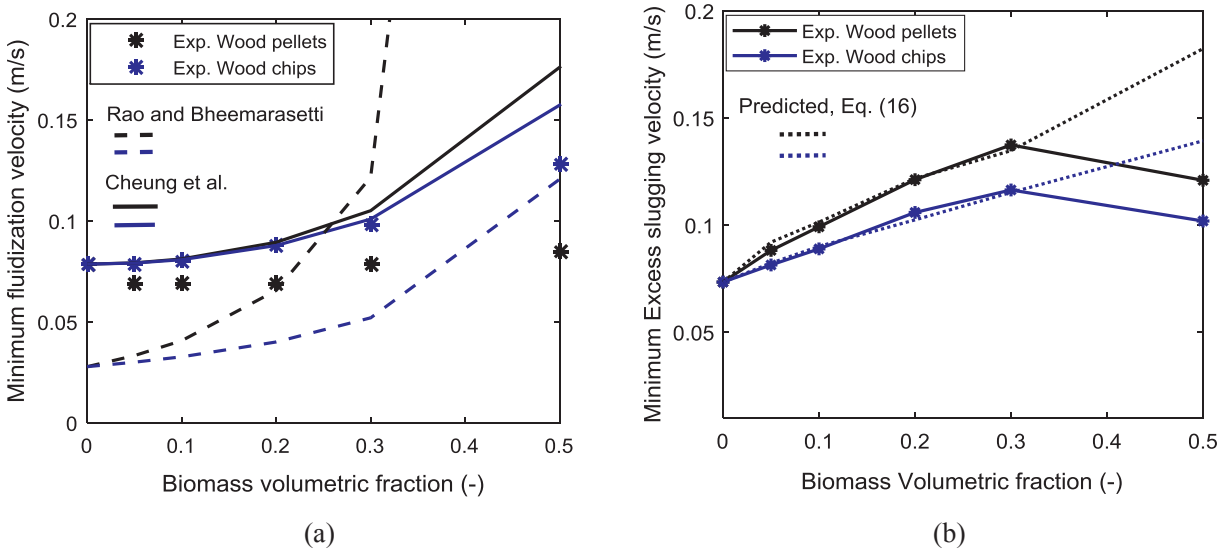


**Fig. 4.** Effect of biomass load on the transition velocity (a) minimum fluidization velocity (b) minimum excess slugging velocity.

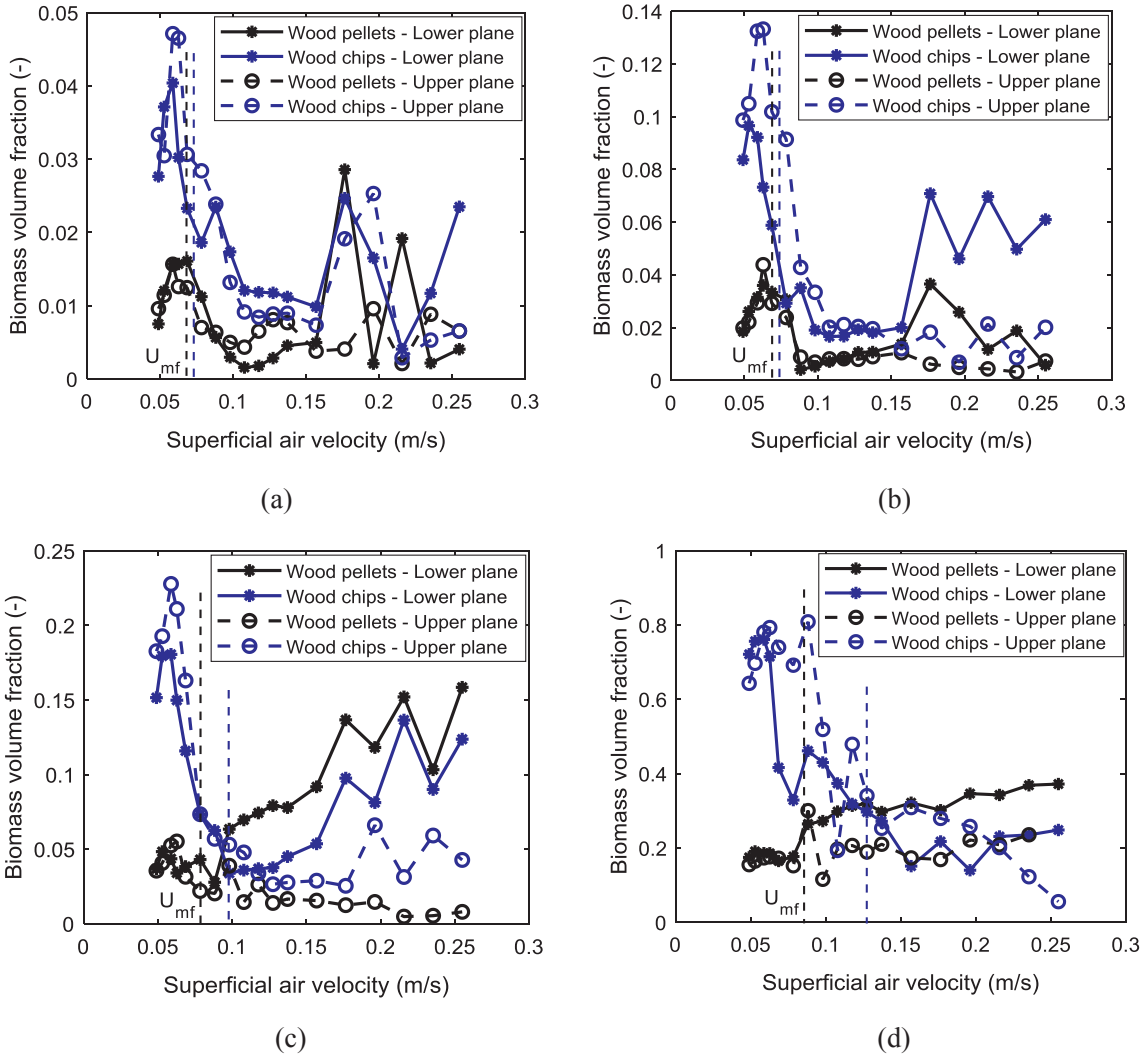


**Fig. 5.** Distribution of biomass particles along the bed for different amount of biomass (a) 10% (b) 20% (c) 30% (d) 50% by volume. Dotted vertical lines demarcate fixed bed from fluidized bed conditions (blue = wood chips; black = wood pellets).

while the Davidson and Harrison [30] model is applied for the bubble velocity, $u_b$. The results from Eq. (17) are compared with those obtained in this study based on Eq. (12).

Fig. 5 shows the variation of average concentration of biomass at different superficial air velocities computed based on Eq. (12) at both measurement planes. With increase in the gas velocity below the minimum fluidization velocity, $U_0 < U_{mf}$ (indicated by the vertical lines), the results show that the biomass concentration increases. Since the column walls were shaken to ensure that the sand particles properly fill up the void of the wood particles during calibration, a larger amount of sand particles was contained in the wood void than should be in a loosely packed state. Therefore, as air flows into the bed, sand particles flow out of the void of the wood particles, increasing the biomass concentration at the measurement planes. The higher concentration of wood chips compared to that of wood pellets at the same measurement position indicates that a larger amount of sand particles flows out in the bed with wood chips. The biomass concentration increases up to a peak value. The peak concentration attained below the bed minimum fluidization velocity increases with the amount of biomass charged into the bed. When the air velocity is slightly above that at the peak concentration, the sand particles become fluidized, leading to segregation of biomass and sand particles. The biomass particles move upwards (in the wood chips case) and downwards (in the wood pellets case), resulting in a reduction in the wood particle concentration at the measurement planes. The upward movement of wood chips at increasing gas velocity can be slightly seen in Fig. 5 since the wood concentration at the upper plane is higher than that at the lower plane when the gas velocity is increased up to the value $U_0 = U_{mf}$. For the case with pellets, Fig. 5(c and d) clearly shows that the concentration of the biomass particles increases down the bed. It should be noted that the two measurement planes are within the middle of the bed. Therefore, only a fraction of biomass in the bed is detected in each of the planes. When the entire bed is fluidized, i.e. $U_0 > U_{mf}$, further segregation occurs due to flow of gas bubbles at low gas velocity, but the rate of segregation at this stage is lower than that at the initial stage. At a higher gas velocity, the biomass particles move back into the bed due to circulation of sand particles from the top to the bottom of the bed.

The degree at which biomass sinks increases with the amount of biomass in the bed and as can be seen, this is more severe with the bed containing wood pellets due to their higher bulk density, which increases with increase in biomass load at a given plane. For example, at $y_b = 0.3$, the concentrations of pellets and chips in the lower plane increases when $U_0 > U_{mf}$, but in the upper plane, the amount of wood pellets decreases while that of wood chips increases at the increasing gas velocity. This indicates that most of the pellets are below the lower plane, and partially a good amount of wood chips is above the upper measurement plane. Similarly, this behaviour can also be observed at $y_b = 0.5$, but within the range of gas velocities shown, the wood chips are still segregated upwards. The higher concentration of biomass at the top or bottom forms a dense layer, which prevents the circulation of sand particles and thus the flow of biomass particles into the bed.

Comparing with the results from Eq. (17), the model predicts a continuous decrease in the concentration of wood chips and pellets in their respective beds at both measurement positions. At some gas velocities, $U_0 - U_{mf} < 0.1$ m/s, and biomass loads, $y_b > 0.2$, the model gives unrealistic results, i.e. $Y_b > 1$. In addition, the predicted biomass volume fractions at the measurement planes are also larger than unity when the total bed height 50 cm is used in the computation for all values of $U_0 - U_{mf}$. This implies that Eq. (17) may be suitable only for higher gas velocities, $U_0 - U_{mf} > 0.3$ m/s, and for a shallow bed, $h_0/D \leq 1.5$, since these are the conditions the authors used in the model validation.

### 3.3. Influence of bubble flow on biomass distribution

Fig. 6 shows the distribution of biomass particles computed from Eq. (11) across the bed for three different gas velocity ratios, $U_0/U_{mfs}$, where $U_{mfs}$ is the minimum fluidization velocity of the sand particles given in Table 1, and for four different biomass fractions at both measurement planes. The value shown is the average of the concentrations at the positions in both x and y axes of the bed. As can be seen, the distribution of biomass particles depends on the gas velocity and on the amount of biomass charged into the bed. Moreover, the pattern of the distribution differs between the two different types of biomass particles.

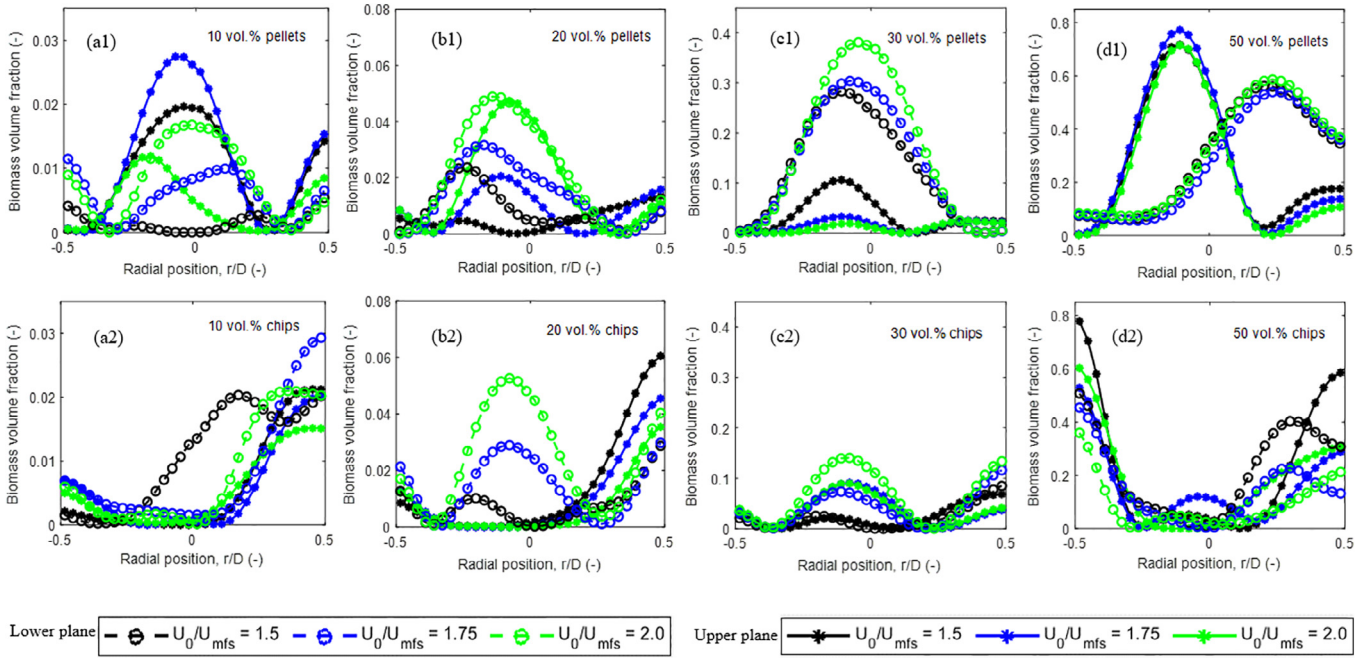


**Fig. 6.** Radial distribution of biomass in a bed mixture with sand particles, comparing the behaviour of wood pellets with that of wood chips at the same gas velocities and biomass loads.

### 3.3.1. Radial distribution of wood pellets and chips

When no bubbles flow in the bed, the biomass concentration attains a peak value at a position between the central axis and the walls. For example at $U_0/U_{mfs} = 1.5$, no bubbles flow in the lower plane of both beds shown in Fig. 6(a1 and a2). Without flow of bubbles, larger amount of sand particles near the walls flow up the bed, resulting in a higher biomass concentration at the walls than at the bed axis. With flows of bubbles, the biomass particles move round in the bed. The wood pellets tend to move towards the central axis while the chips spread to the walls at the same gas velocity due to circulation of sand particles across the segregated biomass layer formed near the bottom (for the former) and near the top (for the latter). The sand particles moving downwards along the bed walls push the wood chips into the bed, increasing the biomass concentration around the walls. In the bed of 20% wood pellets, sand particles push the biomass into the bed along the central axis as they move upwards with the rising bubbles while in that of higher biomass loads, the pellets sink along the path of bubble flows, resulting in a higher biomass concentration at the central axis. The lower concentration of biomass near the walls is due to downward flow of sand particles, and as can be seen in Fig. 6(a1–c1), the wall region with little amount of biomass particles increases from the lower to the upper plane. In addition, the spread of biomass towards the walls decreases down the bed and with an increase in the gas velocity due to increased sand particle circulation at higher gas velocities. The tendency of wood chips to move towards the bed centre increases with increasing biomass load and increasing gas velocity.

In the bed containing 50% pellets as shown in Fig. 6(d1), the lower region of the bed is not fluidized at the given gas velocities due to accumulation of the biomass and thus no flow of bubbles. At the upper plane, the biomass layer interfaces with the fluidized sand particles above. The biomass concentration is high in this plane since sand particles constantly leave the plane and no circulation through the layer below. At the walls, sand particles tend to penetrate through the biomass layer, leading to a reduced biomass concentration near the walls. In the bed with wood chips, bubbles flow in the lower plane when $U_0/U_{mfs} > 1.75$ and in the upper plane when $U_0/U_{mfs} > 1.5$. Due to these low gas velocities shown in Fig. 6(d2), the bubble-induced biomass movement is insignificant in the bed of wood chips. The higher concentration of chips at the wall region makes it difficult for sand particles to penetrate to the bottom of the bed, thus preventing rise of wood chips along the central axis.

### 3.3.2. Vertical distribution of wood pellets and chips

For the loads $y_b < 0.5$, the concentrations of biomass in the lower plane increase with an increase in the gas velocity as shown in Fig. 6(a–c). In Fig. 6(a1), the pellet concentration is higher in the upper plane than in the lower plane due to low bulk density of the biomass particles, which reduces the tendency of the particles to sink into the bed at this load. Increasing the gas velocity to $U_0/U_{mfs} = 2$ , the higher circulation of sand pushes the biomass particles down into the bed, resulting in a higher concentration in the lower plane than in the upper plane. With $y_b = 0.2$, the wood pellets from the lower region of the bed move upwards, increasing the concentration of the biomass particles in the upper plane as the gas velocity is increased. However, in the bed with 30% wood pellets, the biomass particles are still segregating downwards even at the gas velocity, $U_0/U_{mfs} = 2$. Increasing the gas velocity increases the sinking of the biomass into the lower bed region, thereby decreasing the concentration of biomass in the upper region as can be seen in Fig. 6(c1). As the biomass particles sink, they form a thick layer, which prevents the flow of sand particles to the bottom of the bed. To breakdown the biomass layer, a higher gas velocity is required to induce a higher sand circulation effect from the surface of the bed. It should also be noted that in a gasification reactor, the extent to which pellets sink may decrease due to reduction in the biomass density as it devolatilizes.

For the bed of wood chips where $y_b < 0.5$, the biomass concentration increases in the lower plane and decreases in the upper plane due to higher degree of biomass sinking as sand circulation becomes vigorous at higher gas velocities. The distribution of wood chips along the bed axis is less symmetrical for $y_b = 0.2$ compared to that when $y_b = 0.3$, and as shown in Fig. 6(b2), little or no chips are in the upper plane near the central axis. This suggests that as bubbles grow larger and rise along the bed, they push the low concentrated biomass particles towards the walls. Moreover, it can also be seen in Fig. 6(c2) that wood chips move into the bed from the top segregated biomass layer at the same gas velocities at which the pellets are still segregating downwards. However, since the concentration of biomass up to the middle of the bed is low even at $U_0/U_{mfs} = 2$, it shows that a significant amount of wood chips is still at the bed surface.

These results therefore show that with a higher biomass load, $y_b > 0.2$, more than twice the minimum fluidization velocity of the bed material is required to overcome the segregation of the biomass particles, thereby achieving a good distribution across the bed height. This is an important point for consideration in a bubbling fluidized bed biomass gasification, which is often carried out at $U_0/U_{mfs} \approx 2$.

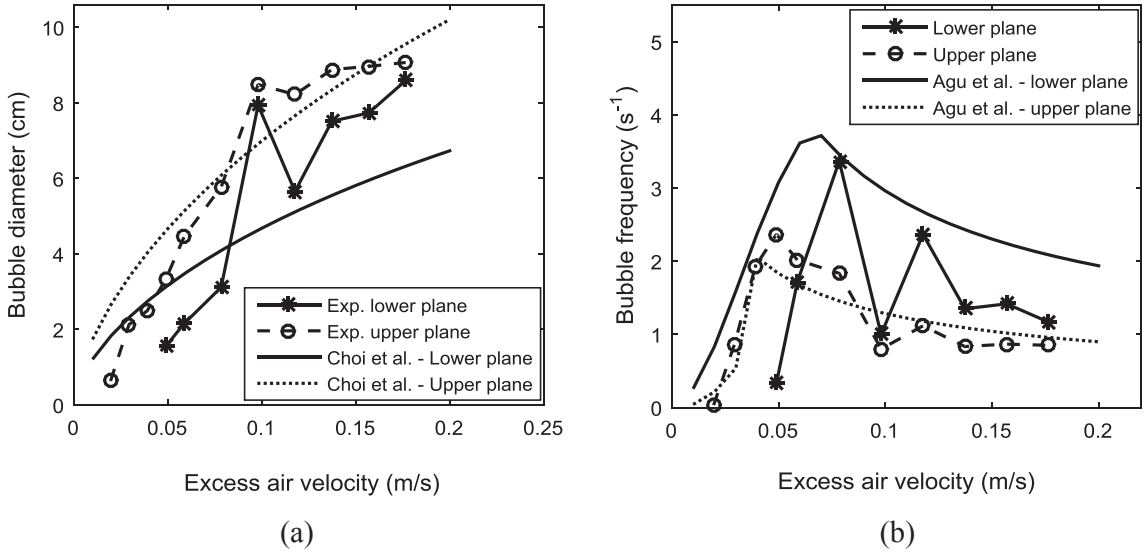


**Fig. 7.** Variation of (a) bubble diameter (b) bubble frequency in a bed of 293 μm sand particles.

### 3.4. Bubble frequency and diameter

Bubble frequency measures the rate of generation of bubbles at a given gas velocity and it depends on the bubble diameter and the rise velocity [31]. No correlation is available for prediction of bubble frequency in a binary mixture of particles. For the bed of pure sand particles, the correlation given in Agu et al. [31] is applied. Similarly, no correlation for bubble diameter is available for a mixture of biomass particles and inert particles, but a number of correlations are available [32] for pure solid particles.

Fig. 7 shows the bubble diameter and bubble frequency for the bed of 298 μm sand particles at different excess air velocities. The bubble diameter increases with increase in the value of $U_0 - U_{mf}$ and along the bed height. The rate of increase in bubble diameter with gas velocity increases at the transition between bubbling and slugging regimes $0.075\ \text{m/s} < U_0 - U_{mf} < 0.1\ \text{m/s}$, but decreases as the bed slugs. This behaviour is typical of beds containing non-spherical (angular) particles [31], which also characterizes the sand particles used in this study. Fig. 7(a) also shows that using the Choi et al. [33] model, the bubble diameter is over-predicted in the bubbling regime and under-predicted in the slugging regime, although the model fits better at the upper part of the bed.

The bubble frequency increases up to a peak value and then decreases as the gas velocity increases. The peak of the bubble frequency indicates a transition to slugging regime, and the gas velocity at which this occurs decreases along the bed height. Below the peak frequency, the change in bubble rise velocity for a unit change in gas velocity (or bubble size) is higher, resulting in an increase in the number of bubbles flowing per unit time as gas velocity is increased [31]. When the bubble size is larger than that at the maximum frequency, the frequency decreases due to the longer time it takes the bubble to pass the given plane. Fig. 7(b) also shows that the Agu et al. [31] model predicts the bed behaviour in the upper plane with a good accuracy. The bubble diameter used in this model is based on the Choi et al. [33] correlation. With the bigger and smaller bubble diameters obtained from the Choi et al. model at gas velocities below and above the peak frequency, respectively, the predicted bubble frequency is significantly higher in the lower plane.

For the mixtures of sand and wood particles, Fig. 8 shows that with an increase in the amount of biomass, the bubble diameter increases in the bubbling regime and decreases in the slugging regime. The vertical lines given in the figures demarcate the bubbling from the slugging regimes. As can be seen, the transition from bubbling to slugging gets smoother as the concentration of biomass in the bed increases. The presence of biomass within the transition region serves as a bubble breaker, preventing rising of large bubbles at high gas velocities as

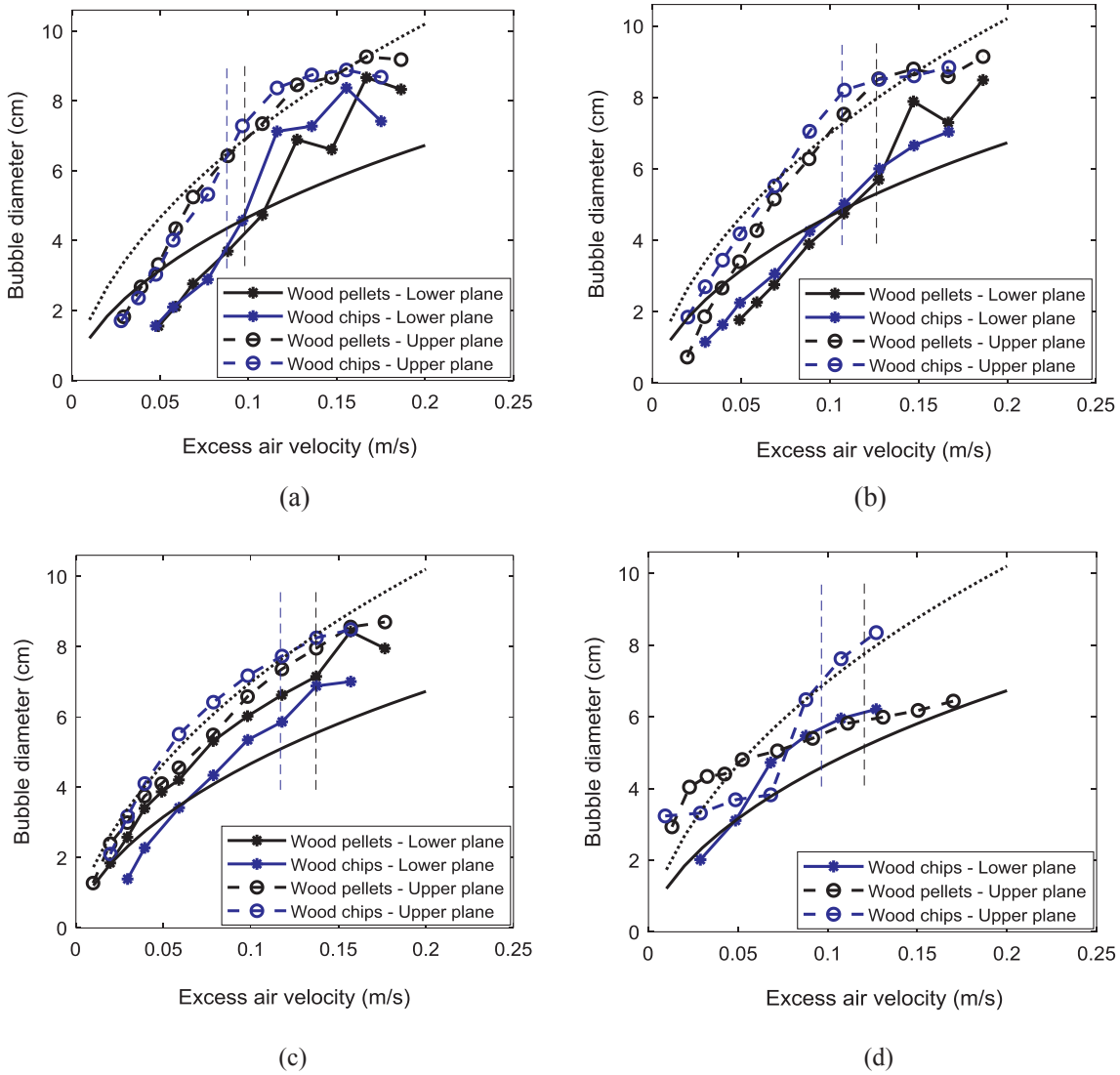


**Fig. 8.** Variation of bubble diameter in a bed mixture of biomass and sand particles for different amount of biomass (a) 10% (b) 20% (c) 30% (d) 50% by volume. Lines: predictions using the Choi et al. [33] model. Dotted vertical lines demarcate bubbling from slugging regimes (blue = wood chips; black = wood pellets).

similarly observed in [11,19]. This therefore explains the results shown in Fig. 4(b) where the minimum slugging velocity increases with biomass load in the bed. At lower amounts of biomass particles, the bubble diameters in both beds are approximately the same at the same measurement position. As the amount of biomass increases, the deviation in the bubble diameters between the two-biomass types increases due to increased accumulation of an un-fluidized layer of biomass. The wood chips layer prevents eruption of bubbles from the top of the bed while the pellet layer prevents fluidization of the bottom region of the bed. When the pellets volume fraction is increased to 0.5, the lower plane becomes de-fluidized due to large amount of biomass particles and thus, no bubbles rise from the bottom of the bed within the range of gas velocities shown.

Fig. 9 shows that the bubble frequency increases with increasing amounts of biomass particles and attains a peak value similar to the case of pure sand particles. The higher bubble frequency indicates that a higher number of bubbles rise through the bed mixture compared to that in the bed of pure sand particles. With a higher bubble frequency, it also suggests that the solids mixing induced by bubbles is better when the biomass load is higher. Moreover, the bubble frequency also decreases along the bed height due to bubble coalescence as similarly shown in Fig. 7(b). The gas velocity at the peak frequency decreases with the biomass load in the bed. At gas velocities above the peak frequency, the bubble frequency is higher in the bed containing wood pellets compared to that containing an equal volume of wood chips. However, for the bed with 30% pellets, the higher concentration of biomass in the lower plane reduces the rate at which bubbles rise through the lower part of the bed, resulting in a lower bubble frequency as shown in Fig. 9(a) and a larger bubble size as can be seen in Fig. 8(c) compared to those of wood chips at the same bed position.

### 3.5. Bed expansion

From the measured bed height at each gas velocity, the bed expansion in the fluidized state is evaluated from $\Delta e = (H_f - H_{mf})/H_{mf}$, where $H_{mf}$ and $H_f$ are the total bed heights from the distributor measured at the minimum fluidization velocity and at a higher gas velocity, respectively. Based on the mass balance of solids and that of gas in the bubble and emulsion phases at different gas velocities, the bed expansion, $\Delta e$ can be computed from

$$\Delta e = \frac{1}{1-\delta_b} - 1 \tag{19}$$

where $\delta_b$ is the average bubble volume fraction defined as

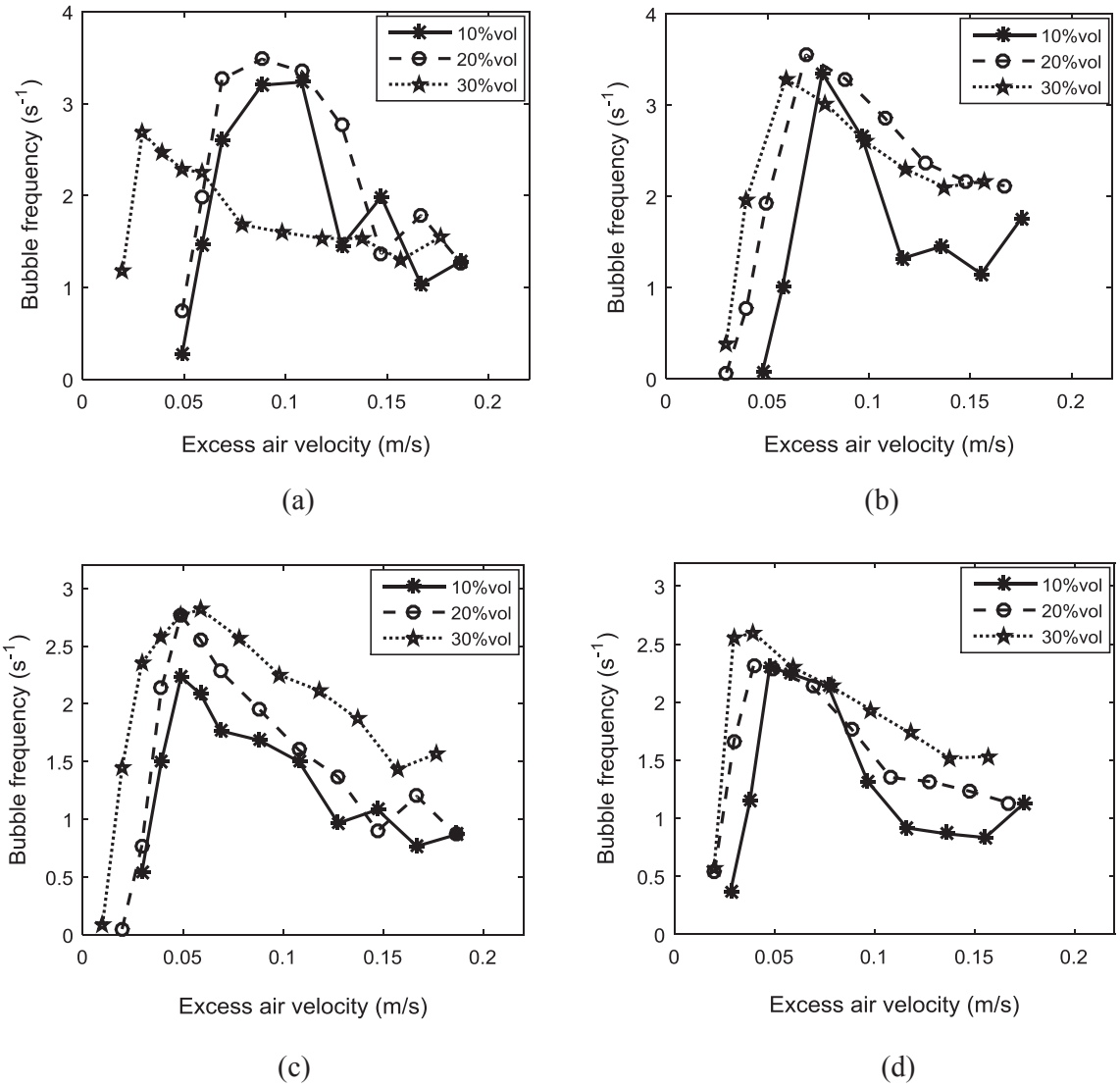


**Fig. 9.** Variation of bubble frequency in a bed mixture of biomass and sand particles at different measurement planes: **Lower plane** (a) wood pellets (b) wood chips. **Upper plane** (c) wood pellets (d) wood chips.

$$\delta_b = G/u_b \tag{20}$$

A value of $\delta_b$ can be obtained using the average bubble velocity, $u_b$ predicted from the available models [30,34,35] and an expression for the bubble volumetric flux, $G$ [23,36]. In addition to Eq. (19), $\Delta e$ can also be predicted using different other correlations [37,38].

Fig. 10 shows the bed expansion measured at air velocity, $U_0/U_{mfS} = 2$ for different biomass loads. In the bed with wood pellets, the bed expansion increases with the biomass load in the range $y_b < 0.2$. For higher biomass loads, the value of $\Delta e$ decreases due to decrease in the volume of bubbles rising through the bed. However, in the bed with wood chips, the total bed expansion (i.e., when the total bed height includes the un-fluidized biomass layer at the surface of the bed) increases with the biomass load up to $y_b = 0.3$ as can be seen in Fig. 10(b) (data points labelled Exp. – total). The higher bed expansion, particularly when $y_b > 0.1$ is due to higher degree of segregation in the bed with wood chips compared to that involving wood pellets. Excluding the top layer containing only the wood chip particles, the bed expansion (indicated as Exp. – fluidized) decreases with increasing amount of biomass. The rapid decrease in the value of $\Delta e$ shows that the dense layer of wood chips at the top of the bed prevents rising of bubbles, thus reducing the bed expansion. In addition, Fig. 10 shows that the predicted results based on the Agu et al. [31] model agree very well with the data obtained in the beds with pellets. With exclusion of the top layer of wood chips, a good agreement with the experimental data is also obtained using the Agu et al. model. The predictions based on the bubble diameter and bubble velocity obtained from the Werther [34] correlations are lower than the experimental data although the predictions get better with increasing amount of biomass in the mixture. Conversely, at a lower biomass load ($y_b < 0.3$), the $\Delta e$ prediction based on the Hepbasli [37] model gives a better result compared to that based on the Werther correlations.

### 3.6. Non bubbling layer – theoretical explanation

Understanding the mechanism behind the accumulation of biomass particles at either the top or bottom of the bed will help in selecting the right parameters during operation and design. For wood chips, the thickness of the top layer increases to a maximum height (observed to be within one-half of the biomass bulk volume in the total mixture) as the gas velocity is increased. While the layer is built up, the bubble eruption at the top of the bed is interrupted. When the solids fraction of the wood layer is close to the solids fraction of the pure biomass in a fixed state, walls act against the bed, preventing further rising of bubbles and penetration of sand particles to the surface of the bed. Increasing the gas velocity above that required for the maximum layer thickness, the particle impact on the layer increases. At a certain velocity, the total force exerted on the biomass layer becomes sufficiently high to overcome the wall frictional force, resulting in penetration of sand particles across the layer and induction of solids circulation at the top of the bed. This mechanism is very important for a hot bed reactor since properties of biomass change at elevated temperature.

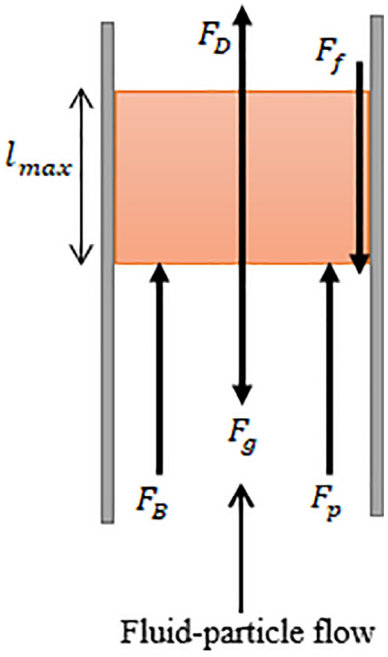


**Fig. 11.** Layer of biomass on the surface of a bed subjected to forces. $F_g = \varepsilon_b \rho_b g A l_{max}$, $F_f = \tau_w \pi D l_{max}$, $F_p = \varepsilon_b \Delta p_g A$, $F_B = (\rho_g + \varepsilon_s f_{wake} \rho_s) G u_b A$, $F_D = \beta A l_{max}$.

For the case of wood pellets, which segregate downwards in the cold flow, the segregation pattern may be reversed in the hot flow reactor due to devolatilization effect. Depending on the heating rate and final temperature, devolatilization can lead to a decrease in the bulk density of the particles [39]. The lower the biomass bulk density, the higher the tendency to move up the bed surface. The upward segregation of biomass in a hot fluidized bed may also be influenced by flow of bubbles

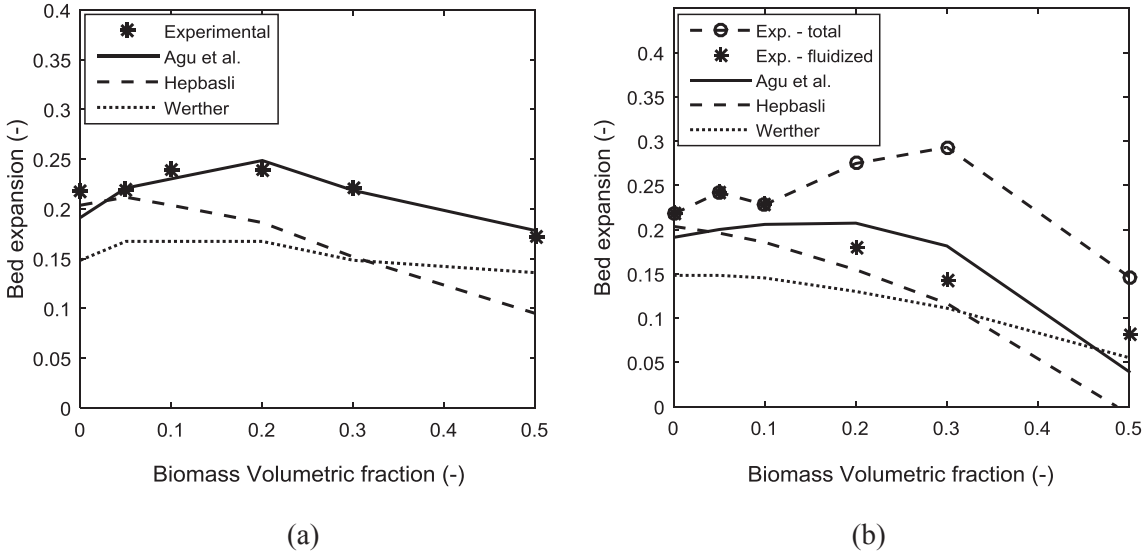


**Fig. 10.** Variation of bed expansion with different biomass loads at $U_0 = 2U_{mfS}$ (a) Wood pellets (b) Wood chips.

around the biomass as it devolatilizes [40], but since the devolatilization time for pellets is relatively small, the effect of volatile bubbles may be less severe [41].

From this observation, it follows that at any given gas velocity, there is a certain maximum thickness of the top layer beyond which there will be no solids circulation. In this section, a simple mathematical model is established to quantify the maximum thickness of a wood layer on the surface of a bed at a given gas velocity. Fig. 11 shows the forces acting on the biomass layer along the flow axis.

By force balance across the biomass layer,

$$\varepsilon_b\rho_b g A l_{max} + \tau_w \pi D l_{max} = \varepsilon_b \Delta p_g A + \beta A l_{max} + (\rho_g + \varepsilon_s f_{wake}\rho_s) G u_b A \tag{21}$$

where $\tau_w$ is the wall stress, $\varepsilon_s$ is the sand solids fraction, $f_{wake}$ is the bubble wake fraction, $\beta$ is the fluid-particle momentum transfer coefficient and $\varepsilon_b$ is the solids fraction of the biomass layer with thickness $l_{max}$. The expression in the right hand side is the total force transferred due to fluid pressure, gas-solid momentum exchange and impingement of bubble and sand particles carried in the wake of the bubble. The left hand side is the total resistance force due to weight of the layer and wall friction. The fluid pressure drop $\Delta p_g$ across the layer can be modelled as

$$\Delta p_g = \gamma \delta_b \varepsilon_s \rho_s g l_{max} \tag{22}$$

Here, $\gamma$ accounts for the effect of non-hydrostatic pressure distribution and non-uniformity of pressure across the bed cross section. For simplicity, $\gamma$ can be assumed the same as the bed aspect ratio corresponding to the bed material. Thus, $\gamma = (1 - y_b)h_0/D$, where $h_0$ is the initial bed height. Applying Columb's law, the wall frictional stress can be obtained as $\tau_w = \mu_w \sigma$, where $\mu_w$ and $\sigma$ are the coefficient of friction and the average normal stress induced on the wall due to internal stress in the wood layer, respectively. The value of $\sigma$ for a given powder strongly depends on the voidage of the powder. When $\varepsilon < \varepsilon_{mf}$, the normal stress has negligible effect on the flow of the powder. For a dense powder flow, different models for $\sigma$ can be found in the literature [42–44]. Based on the model given by Rankine [44], a value of $\sigma$ can be predicted from

$$\sigma = \frac{1}{2}\varepsilon_b \rho_b g l_{max} k \tag{23}$$

$$k = \left(\frac{1 - sin\theta_i}{1 + sin\theta_i}\right)$$

Here, $k$ is the pressure coefficient and $\theta_i$ is the angle of internal friction in the wood layer.

Substituting Eqs. (22 and 23) in Eq. (21), gives

$$\varepsilon_b\rho_b g A l_{max} + \frac{2}{D}\mu_w k \varepsilon_b \rho_b g {l_{max}}^2 A = \gamma \varepsilon_b \delta_b \varepsilon_s \rho_s g A l_{max} + (\rho_g + \varepsilon_s f_{wake}\rho_s) G u_b A + \beta A l_{max}$$

$$\frac{2}{D}\mu_w k {l_{max}}^2 + (1 - \gamma\frac{\rho_s}{\rho_b}\delta_b\varepsilon_s - \frac{\beta}{\varepsilon_b\rho_b g}) l_{max} = \frac{(\rho_g + \varepsilon_s f_{wake}\rho_s)}{\varepsilon_b g \rho_b} G u_b \tag{24}$$

For the application of Eq. (24), all the bubble properties are computed at the bed position near the bottom of the biomass layer, i.e. $h = (0.5y_b + 1)h_0$. To obtain the minimum gas velocity required to achieve solids mixing at the surface of the bed, $l_{max} = 0.5y_b h_0$ is used. The bubble diameter, bubble velocity and bubble volumetric flux can be estimated as respectively proposed by Werther [34], Davidson and Harrison [30] and Kunii and Levenspiel [36].

$$D_b = 0.853[1 + 0.272(U_0 - U_{mf})]^{1/3}(1 + 0.0684h)^{1.21}, \quad [\text{cm}] \tag{25}$$

$$u_b = U_0 - U_{mf} + 0.711(gD_b)^{0.5} \tag{26}$$

$$G = \varnothing(U_0 - U_{mf}); \ \varnothing = 0.65 \tag{27}$$

Fig. 12 illustrates the application of Eq. (24) for determining the minimum gas velocity required to achieve solid circulation at the top of a bed containing wood chips. The mean values of the frictional parameters, $\theta_i$ and $\mu_w$ used are 45° and 0.35, respectively as reported in [45], and the bubble wake fraction $f_{wake}$ for the 293 μm sand particles is 0.24 [36]. The momentum transfer coefficient $\beta = 0$ is assumed since the size of the biomass particles is very large and the gas velocity at the operating condition is far below the minimum fluidization velocity of the wood particles. The increase in the thickness of the biomass layer as the gas velocity increases is shown in Fig. 12(a) for the bed of diameter 10.4 cm and aspect ratio of 5.0. As can be seen, the maximum thickness of the layer increases with the amount of wood particles in the bed. The minimum excess gas velocity, $U_0 - U_{mf}$, before bubbles can erupt from the bed surface also increases with biomass load. Moreover, the predicted gas velocity from Eq. (24) at the maximum thickness of the wood layer (approximated to $0.5y_b h_0$), agrees with the experimental data. The predicted results also show that solids mixing at the top of the bed containing 5% biomass occurs when $U_0 - U_{mf} \approx 0.045$ m/s. For the mixture with 50% biomass, the predicted minimum value of $U_0 - U_{mf}$

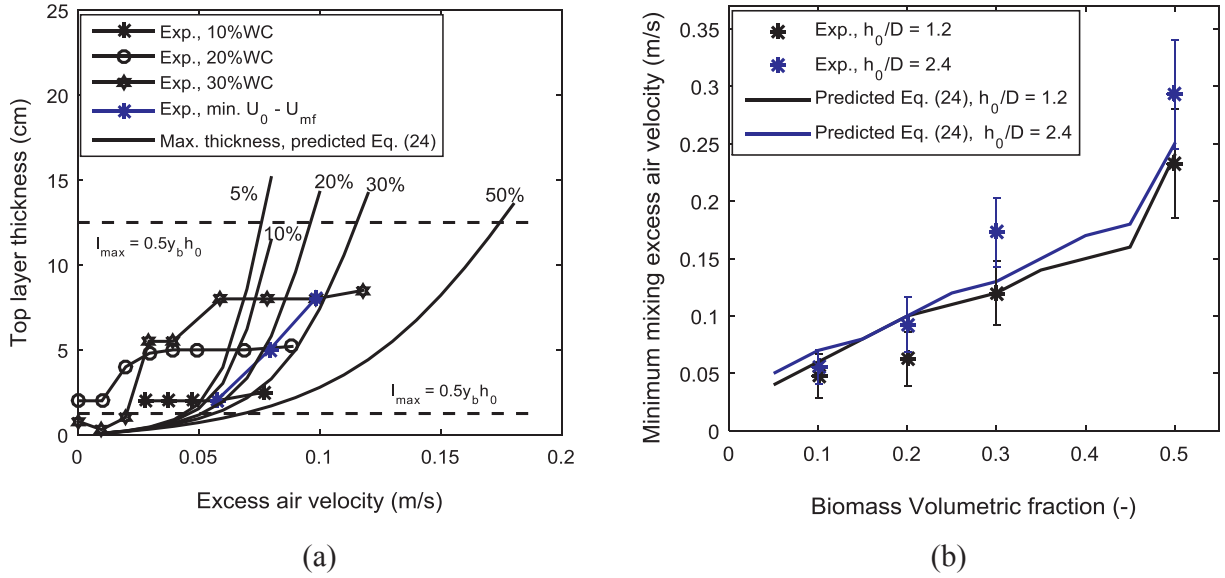


**Fig. 12.** (a) Variation of thickness of wood chip layer at the bed surface showing minimum gas velocity for particle mixing in the bed; $D = 10.4$ cm and $h_0/D = 5$. (b) Variation of minimum gas velocity for particle mixing with wood chips load in the bed; $D = 8.4$ cm at different aspect ratios, $h_0/D = 1.2$ and $h_0/D = 2.4$.

for the top mixing is 0.175 m/s. However, below this velocity, the bed is slugging as shown in Fig. 4, making it difficult to achieve the right mixing in this deep bed. Decreasing the bed height reduces the chances of slugs flow in a bed. The range of gas velocities required to break through the top layer and achieve a continuous mixing are shown in Fig. 12(b) for different biomass loads. The results are obtained in the bed of 8.4 cm at two different aspect ratios, $h_0/D = 1.2$ and $h_0/D = 2.4$. The error bar represents the range of gas velocity at which a complete mixing of particles was observed at the top of the bed while the data point represents the mean value of these velocities. As can be seen, the mean gas velocity increases with increase in the aspect ratio. However, the overlap in the range of velocities between the two aspect ratios shows that the bed height may have insignificant effect on the gas velocity required to achieve a continuous mixing at the surface of the bed. The figure also shows that the predicted results based on Eq. (24) agree with the experimental data within the range of observed values. The minimum values of $U_0 - U_{mf}$ predicted for different biomass concentration also vary slightly with changes in the bed aspect ratio. Comparing the results shown in Fig. 12(a and b), the excess gas velocity to achieve the solids mixing decreases with increased bed diameter, which may be due to the decrease in the wall frictional force as the bed diameter increases. From these results, it follows that Eq. (24) properly accounts for the mechanism in breaking down the top layer of biomass to achieve continuous mixing, and can be used to predict the minimum gas velocity required to achieve mixing of solid particles in binary mixtures.

## 4. Conclusion

This study investigated the segregation pattern and bubbling properties in cold fluidized beds containing mixtures of sand and biomass particles using measured ECT data obtained from a 10.4 cm diameter cylindrical column. The bed behaviour involving wood chips of irregular shape and low density are compared with those involving cylindrical wood pellets of higher density.

The results showed that at low gas velocity, the wood chips segregate upwards while the wood pellets segregate downwards in their respective beds. The degree of segregation increases with biomass load. The segregation behaviour at a gas velocity below the bed minimum fluidization is more severe in the case with wood chips, resulting in a steady increase in the minimum fluidization velocity compared to the case with wood pellets, which shows a negligible change in the minimum fluidization velocity up to a biomass load of 50% by volume. The maximum thickness of wood chips accumulated at the bed surface in steady state is about 50% of the height of pure biomass charged into the bed. At higher gas velocities, the biomass particles move back into the bed from the segregated layers. The gas velocity required to achieve mixing over the bed is almost independent of initial bed height, but increases with biomass load and decreases with bed diameter. By a force balance, a mechanistic model was formulated for predicting the minimum gas velocity required to achieve an effective mixing in the bed mixture.

The results also show that both the bubble diameter and bubble frequency increase within the bubbling regime as the amount of biomass increases. The transition from bubbling to slugging regime also gets smoother as the biomass load increases, resulting in an increase in the minimum slugging velocity and a decrease in the bubble diameter within the slugging regime. To successfully scale up this behaviour to a hot bed reactor, the extent to which temperature influences the distribution of biomass particles needs to be investigated.

## 5. Funding sources

This research did not receive any specific grant from funding agencies in the public, commercial, or not-for-profit sectors.

## References

[1] X. Wu, K. Li, F. Song, X. Zhu, Fluidization behaviour of biomass particles and its improvement in a cold visualized fluidized bed, BioResources 12 (2017) 3546.
[2] Y.H. Chen, J. Yang, R.N. Dare, R. Pfeffer, Fluidization of coated group C powders, AIChE J. 54 (2008) 104.
[3] L.F. Zhang, J.T. Hou, X.T. Bi, J.R. Grace, T. Janke, C. Arato, Fluidization characteristics and changing behaviour of fly ash in vibro-fluidized bed, Powder Technol. 215 (2012) 235.
[4] C. Si, Q. Guo, Fluidization characteristics of binary mixtures of biomass and quartz sand in an acoustic fluidized bed, Ind. Eng. Chem. Res. 47 (2008) 9773.
[5] D. Escudero, T.J. Heindel, Minimum fluidization velocity in a 3D fluidized bed modified with an acoustic field, Chem. Eng. J. 231 (2013) 68.
[6] B.T. Vilches, E. Sette, H. Thunman, Behaviour of biomass particles in a large scale (2–4 MWth) bubbling bed reactor, WIT Trans. Eng. Sci. 89 (2015) 151.
[7] T.R. Rao, J.V.R. Bheemarasetti, Minimum fluidization velocities of mixtures of biomass and sands, Energy 26 (2001) 633.
[8] B. Paudel, Z.-G. Feng, Prediction of minimum fluidization velocity for binary mixtures of biomass and inert particles, Powder Technol. 237 (2013) 134.
[9] A.C. Kumoro, D.A. Nasution, A. Cifriadi, A. Purbasari, A.F. Falaah, A new correlation for the prediction of minimum fluidization of sand and irregularly shape biomass mixtures in a bubbling fluidized bed, IJAER 9 (2014) 21561.
[10] A. Di Renzo, F.P. Di Maio, R. Girimonte, V. Vivacqua, Segregation direction reversal of gas-fluidized biomass/inert mixtures – experiments based on Particle Segregation Model predictions, Chem. Eng. J. 262 (2015) 727.
[11] F. Fotovat, R. Ansart, M. Hemati, O. Simonin, J. Chaouki, Sand-assisted fluidization of large cylindrical and spherical biomass particles: Experiments and simulation, Chem. Eng. Sci. 126 (2015) 543.
[12] M. Wirsum, F. Fett, N. Iwanowa, G. Lukjanow, Particle mixing in bubbling fluidized beds of binary particle systems, Powder Technol. 120 (2001) 63.
[13] F. Fotovat, J. Chaouki, J. Bergthorson, Distribution of large biomass particles in a sand-biomass fluidized bed: Experiments and modeling, AIChE J. 60 (2014) 869.
[14] B. Cluet, G. Mauviel, Y. Rogaume, O. Authier, A. Delebarre, Segregation of wood particles in a bubbling fluidized bed, Fuel Process Technol. 133 (2015) 80.
[15] Y. Zhang, B. Jin, W. Zhong, Experimental investigation on mixing and segregation behaviour of biomass particles in fluidized bed, Chem. Eng. Process. 48 (2009) 745.
[16] J. Baeyens, D. Geldart, Solid mixing, in: G. Gelart (Ed.), Gas Fluidization Technology, New York, Willey, 1986, p. 97.
[17] S.C. Yang, Density effect on mixing and segregation processes in a vibrated binary granular mixture, Powder Technol. 164 (2006) 65.
[18] M.J.V. Goldschmidt, J.M. Link, S. Mellema, J.A.M. Kuipers, Digital image analysis measurements of bed expansion and segregation dynamics in dense gas-fluidized beds, Powder Technol. 138 (2003) 135.
[19] Y. Zhang, B. Jin, W. Zhong, B. Ren, R. Xiao, Characterization of fluidization and segregation of biomass particles by combining image processing and pressure fluctuations analysis, Int. J. Chem. React. Eng. 7 (2009) 1.
[20] M. Rudisuli, T.J. Schildhauer, S.M.A. Biollaz, van-Ommen, J.R. Scale-up of bubbling fluidized bed reactors –, A review. *Powder Technol.* 217 (2012) 21.
[21] C.E. Agu, A. Ugwu, C. Pfeifer, M. Eikeland, L.-A. Tokheim, B.M.E. Moldestad, Investigation of bubbling behaviour in deep fluidized beds at different gas velocities using electrical capacitance tomography, Ind. Eng. Chem. Res. (2019), https://doi.org/10.1021/acs.iecr.8b05013.
[22] C.E. Agu, L.-A. Tokheim, M. Eikeland, B.M.E. Moldestad, Determination of onset of bubbling and slugging in a fluidized bed using a dual-plane electrical capacitance tomography system, Chem. Eng. J. 328 (2017) 997.
[23] C.E. Agu, C. Pfeifer, M. Eikeland, L.-A. Tokheim, B.M.E. Moldestad, Models for predicting average bubble diameter and volumetric bubble flux in deep fluidized beds, Ind. Eng. Chem. Res. 57 (2018) 2658.
[24] P.C. Carman, Fluid flow through granular beds, Trans. Inst. Chem. Eng. 15 (1937) 150.
[25] L. Cheung, A.W. Nienow, P.N. Rowe, Minimum fluidization velocity of a binary mixture of different sized particles, Chem. Eng. Sci. 29 (1974) 1301.
[26] J. Baeyens, D. Geldart, An investigation into slugging fluidized beds, Chem. Eng. Sci. 29 (1974) 255.
[27] S. Shaul, E. Rabinovich, H. Kalman, Generalized flow regime diagram of fluidized beds based on the height to bed diameter ratio, Powder Technol. 228 (2012) 264.
[28] L.G. Gibilaro, P.N. Rowe, A model for a segregation gas fluidized bed, Chem. Eng. Sci. 29 (1974) 1403.
[29] R.C. Darton, R.D. La Naueza, J.F. Davidson, D. Harrison, Bubble growth due to coalescence in fluidized beds, Trans. Inst. Chem. Eng. 55 (1977) 274.
[30] J.F. Davidson, D. Harrison, Fluidized Particles, Cambridge University Press, London, 1963.
[31] C.E. Agu, L.-A. Tokheim, M. Eikeland, B.M.E. Moldestad, Improved models for predicting bubble velocity, bubble frequency and bed expansion in a bubbling fluidized bed, Accepted on Nov. 2, 2018 for publication in Chemical Engineering Research and Design.
[32] S. Karimipour, T. Pugsley, A critical evaluation of literature correlations for predicting bubble size and velocity in gas-solid fluidized beds–a review, Powder Technol. 205 (2011) 1.
[33] J.H. Choi, J.E. Son, S.D. Kim, Bubble size and frequency in gas fluidized beds, J. Chem. Eng. Jpn. 21 (1988) 171.
[34] J. Werther, Effect of gas distributor on the hydrodynamics of gas fluidized beds, Ger. Chem. Eng. 1 (1978) 166.
[35] K. Hilligardt, J. Werther, Local bubble gas hold-up and expansion of gas/solid fluidized beds, German Chem. Eng. 9 (1986) 215.

[36] D. Kunii, O. Levenspiel, Fluidization Engineering, Second ed., Butterworth – Heinemann, Washington Street, 1991.
[37] A. Hepbasli, Estimation of bed expansions in a freely-bubbling three-dimensional gas-fluidized bed, Int. J. Energy Res. 22 (1998) 1365.
[38] R.K. Singh, A. Suryanarayana, G.K. Roy, Prediction of bed expansion ratio for gas-solid fluidization in cylindrical and non-cylindrical beds, IE (1) Journal-CH. 79 (1999) 51.
[39] J. Saastamoinen, Release profile of volatiles in fluidised bed combustion of biomass, J. Fundam. Renewable Energy Appl. (2015) 5.
[40] M. Fiorentino, A. Marzocchella, P. Salatino, Segregation of fuel particles and volatile matter during devolatilization in a fluidized bed reactor – II. Experimental, Chem. Eng. Sci. 1997 (1909) 52.
[41] F. Miccio, S. Russo, N. Silvestri, Assessment of the devolatilization behaviour of fuel pellets in fluidized bed, Fuel Process Technol. 115 (2013) 122.
[42] H.A. On Janssen, the pressure of grain in silos, Proceedings of the Institution of Civil Engineers 124 (1896) 553.
[43] M.S. Ketchum, The Design of Walls, Bins and Grain Elevator, third ed., Mc Graw-Hill Book Company Inc., New York, 1919.
[44] W.J.M. Rankine, On the stability of loose earth, Phil. Trans. R. Soc. Lond. 147 (1857) 145.
[45] M.R. Wu, D.L. Schott, G. Lodewijks, Properties of solid biomass, Biomass Bioenergy 35 (2011) 2093.